agronomy

MDPI

Article

CsNWD Encoding VPS62 Emerges as a Candidate Gene Conferring the Glabrous Phenotype in Cucumber

Yuelong Zhou, Mingyuan Xu, Yong Zhou, Zhaoyang Hu and Shiqiang Liu *

College of Bioscience and Bioengineering, Jiangxi Agricultural University, Nanchang 330045, China; zhouyl21@jxau.edu.cn (Y.Z.); 15797794879@163.com (M.X.); yongzhou@jxau.edu.cn (Y.Z.); huzhaoyang@jxau.edu.cn (Z.H.)

* Correspondence: lsq_hn306@163.com

Abstract: The commercial value of cucumbers is influenced by the presence of spines or trichomes on their fruit, while the trichomes found on other parts of the plant are essential for protecting the cucumber against a range of biotic and abiotic stresses. In our research, we identified a glabrous *nwd* mutant from EMS-induced cucumber (*Cucumis sativus* L.) mutant lines. This mutant displays a consistent glabrous phenotype across all plant organs. Upon analysis, it was revealed that the *nwd* mutation is governed by a lone recessive nuclear gene. The *nwd* plants show a significant reduction in both their photosynthetic capacity and chlorophyll a content when compared to the wild-type. Furthermore, there are notable changes in the antioxidant enzyme activities, soluble protein levels, and malondialdehyde content of the *nwd* mutant. Genotyping and MutMap approaches identified the *CsNWD* gene, encoding a VPS protein, as a candidate responsible for the glabrous trait. Transcriptome analysis indicated that 15 trichome-related genes exhibit significant expression changes in the *nwd* mutant, implying that *CsNWD* may regulate trichome development through interactions with these genes. This study contributes to the understanding of VPS proteins in trichome initiation and the underlying mechanisms of trichome development.

Keywords: glabrous; trichome initiation; VPS; cucumber

check for updates

Citation: Zhou, Y.; Xu, M.; Zhou, Y.; Hu, Z.; Liu, S. *CsNWD* Encoding VPS62 Emerges as a Candidate Gene Conferring the Glabrous Phenotype in Cucumber. *Agronomy* **2024**, *14*, 2019. https://doi.org/10.3390/agronomy14092019

Academic Editors: Daniele Antichi, Christian Frasconi and Marco Fontanelli

Received: 22 July 2024
Revised: 29 August 2024
Accepted: 2 September 2024
Published: 4 September 2024

Copyright: © 2024 by the authors. Licensee MDPI, Basel, Switzerland. This article is an open access article distributed under the terms and conditions of the Creative Commons Attribution (CC BY) license (https://creativecommons.org/licenses/by/4.0/).

1. Introduction

Plant trichomes are special accessory structures that differentiate from epidermal cells and cover the surface organs of plants [1]. As the first line of defense, these tiny protrusions serve multiple functions; they not only reduce water evaporation, but also protect plants from biotic and abiotic stresses [2]. Trichomes, whether present or absent, are a crucial determinant of product quality for certain specialty crops like cucumber (*Cucumis sativus* L.).

Cucumber is an important economically cultivated crop throughout the world [3]. The stems, leaves, flowers, branches, fruits, and tendrils of cucumber plants are covered with trichomes [4,5]. The cucumber fruit bears thorns composed of trichomes, with a multi-layer nodulation beneath them [6]. Through histological analysis, it was discovered that the leaf trichomes and fruit-borne prickles unique to cucumbers share a similar morphology and structure: both are multicellular and lack glands, distinguishing them from the single-celled, branched trichomes in Arabidopsis or the various types found in tomatoes [7]. Cucumber trichomes can be categorized into eight distinct varieties: Type I trichomes are composed of a brief, single-file stalk and a head region. Type II trichomes are characterized by their spherical, multicellular base and a stalk that is elongated and made up out of up of six to eight cells. Type III trichomes include a stalk composed of three to six cells that is shorter compared to Type II trichomes, and they end with a pointed tip above a conical base. The appearance of Type IV trichomes is of a shorter stem and a smaller base compared to Type II trichomes. The Type V trichomes are pyramidal in appearance and

have no obvious slender stems and swollen bases. Type VI trichomes have longer stem cells than type I trichomes. Types VII and VIII were found only in the glabrous mutant *csgl1* [7,8]. Cucumber trichomes are closely related to their economic value and resistance to biotic and abiotic stresses [9,10]. Moreover, the characteristics of trichomes, especially those protruding from the fruit surface, play a crucial role in commercial categorization. Specifically, the occurrence, frequency, and dimensions of these fruit-borne projections serve as key indicators for market segmentation [11].

Existing research literature suggests that the fate determination and initiation stages of cucumber trichomes are closely associated with homeodomain-leucine zipper complexes (HD-ZIP), myeloblastosis-related factors (MYB), and zinc finger motifs of the Cys2-His2 variety (C2H2-type) transcription factors, as well as WD-repeat proteins [2]. A subset of genes belonging to the HD-ZIP I family, including *TINY BRANCHED HAIR* (*CsTBH*), *GLABROUS 1* (*CsGL1*), and *MICRO-TRICHOME* (*CsMICT*) are involved in the formation of cucumber trichomes [6,8,12]. On the surface of leaves with the *csgl1* mutation, numerous papillae are observable, with a density consistent with wild-type cucumbers, suggesting that *CsGL1* could be involved in leaf trichome development, rather than fate determination and initiation [6]. The down-regulation of *CsMYB6* in *csgl1* suggests its potential significance in the development of foliar trichomes and fruit spines in cucumber. Moreover, *CsGA20ox1*, encoding a pivotal biosynthetic enzyme involved in the production of gibberellic acids (GAs), is up-regulated in *csgl1*. When *CsGA20ox1* is overexpressed, it results in the formation of shorter fruit spines as compared to the wild-type, indicating that CsGA20ox1 acts as a suppressor in regulating the growth of cucumber fruit spines [6]. The phenotypes of the alleles of *CsGL1*, namely the *mict* and *tbh* mutants, exhibit trichome characteristics similar to those of the *CsGL1* mutant. All the leaves and fruit trichomes in the *mict* mutant are small and stunted [13,14]. The induction of spine dysplasia was observed in wild-type plants upon the silencing of *CsTBH*. Interestingly, there seems to be no direct involvement of *CsTBH* in the initiation of spines [7,8]. Mutant phenotypic analysis has indicated that *CsTBH*, *CsMICT*, and *CsGL1* participate in the regulation of glandular hair morphogenesis, rather than being responsible for determining or initiating their fate.

TRICHOME-LESS (*Tril*) and *CsGL3*, which belong to the HD-ZIP IV family, have been identified as key players in the fate determination and initiation of trichomes in cucumber. The mutations of these two genes show glabrous stems, leaves, sepals, flowers, and fruits [6,15,16]. The *csgl2* mutant shows glabrous stems and leaves, but few trichomes on the calyx, tendrils, ovary, and fruit [17].

The cucumber fruit spine initiation negative regulators *CsMYB6* and *CsTRY* belong to the MYB-type transcription factor family. Significant inhibition of leaf trichome development is observed in Arabidopsis thaliana upon the expression of *CsTRY*, indicating a potential inhibitory role of the *CsTRY* gene in cucumber trichome development [18,19]. *CsGL1* exhibits an epistatic effect on *Tu*, emphasizing its importance as a regulatory factor in controlling fruit tumor formation alongside the C2H2 zinc finger protein gene *Tu* [17,20]. The formation of fruit thorns is inhibited by the silencing of the WD-repeat protein gene *CsTTG1* [21].

2. Materials and Methods

2.1. Plant Materials, Conditions for Growth, and the Identification of Phenotypes

A stable glabrous mutant, *nwd*, was isolated from an EMS-mutagenized population of wild-type cucumber (HB, Southern China type). The HB variety was used as the control for comparison. Cucumber plants were cultivated in a greenhouse under long-day conditions, with 16 h of light and 8 h of darkness, at a temperature range of 22–25 °C. The growth medium consisted of a 1:3 mixture of fertile soil and vermiculite, with weekly nutrient solution irrigation. LED lamps provided a light intensity of 300 $\mu mols \cdot m^{-2} \cdot s^{-1}$, maintaining humidity between 75 and 85%. Observations of trichomes and fruit thorns were conducted on 30 plants post-seed germination. Using a measuring tape, the plant height, leaf length, leaf width, stem diameter, and petiole length of the true leaves were

measured during the seedling, vine, and maturity stages. ImageJ (V1.8.0) software was utilized to determine the leaf area from photographs.

2.2. Genetic Analysis

Self-pollination of the glabrous mutant *nwd* over five generations resulted in a consistent manifestation of the glabrous phenotype. The inbred line HB (P_1) was chosen as the maternal parent due to its significant phenotypic difference in trichomes compared to *mwd* (P_2). To determine the inheritance pattern of the glabrous gene (*nwd*), populations including 11 F_1, 106 BC_1P_1, 106 BC_1P_2, and 152 F_2 were generated. Statistical analysis of glabrous phenotypes in the F_2 population occurred post-maturation of the third true leaf. The occurrence of the wild-type and glabrous phenotype among plants was analyzed using the $\chi 2$ test.

2.3. Transpiration Rate, Net Photosynthetic Rate, and Chlorophyll Content Determination

The CI-340 Handheld Photosynthesis System (manufactured by CID, United States) was used to evaluate the transpiration rate and net photosynthetic rate for both the *nwd* mutant and WT plants on a sunny day. The net photosynthetic rate reflects the carbon dioxide absorption. Three leaves with similar growth and positions from both the *nwd* mutant and wild-type plants were measured between 9:00–11:00 a.m.

Under identical growth conditions, the levels of chlorophyll a, chlorophyll b, total chlorophyll (photosynthetic pigment), and carotenoid contents were quantified [22]. Fresh leaves from the third true leaf of both *nwd* and HB plants were selected for chlorophyll extraction. Approximately 200 mg of leaves were placed into 15 mL tubes containing a mixture of acetone, ethanol, and ddH_2O (in a volume ratio of 4.5:4.5:1) and kept in the dark for two days at 4 °C. Following centrifugation, the supernatant was gathered, and the concentrations of chlorophyll a, chlorophyll b, and carotenoids were measured with a UV-visible spectrophotometer (UV-6800, 7G, Qingdao, Tianjin, China) at absorbance wavelengths of 665 nm, 649 nm, and 470 nm, respectively. Chlorophyll and carotenoid were calculated with the following formula: chlorophyll a = $(13.95 \times OD_{665} - 6.88 \times OD_{649}) \times V/(1000 \times W)$; chlorophyll b = $(24.96 \times OD_{649} - 7.32 \times OD_{665}) \times V/(1000 \times W)$; Chl = $(6.63 \times OD_{665} + 18.08 \times OD_{649}) \times V/(1000 \times W)$; carotenoid = $(1000 \times OD_{470} - 2851.304 \times OD_{649} + 811.7385 \times OD_{665})/245$. V: volume of extraction solution, W: sample weight.

2.4. Antioxidant Enzyme Activity Determination

Superoxide dismutase (SOD), peroxidase (POD), and catalase (CAT) activities were assessed in three randomly selected leaves at corresponding stages of development, both in *nwd* mutant and wild-type seedling and vine stages. The activity levels of SOD and CAT were determined using assay kits provided by the Nanjing Jiancheng Bioengineering Institute (http://mall.njjcbio.com (accessed on 1 May 2024); A001-3-2). For POD activity determination, the following solution was added to the wells of a 96-well enzyme-labeled plate: 50 µL of the supernatant from the SOD activity determination mixed with 20 µL of 1% guaiacol prepared in 0.05 M PBS, followed by the addition of 20 µL of 0.05 M PBS (pH = 6.5), and finally, 20 µL of 0.2 mol/L H_2O_2. The mixture was allowed to react for exactly 2 min, with readings taken every 30 s at 470 nm. A blank control was used with PBS (0.05 M, pH 6.5) instead of the enzyme solution.

2.5. Soluble Sugars, Malondialdehyde (MDA), and Electrical Conductivity Analysis

The determination of soluble protein content was referenced from the Coomassie Brilliant Blue G-250 staining method [23], and the determination of soluble sugar content was referenced from the anthrone colorimetric method. For malondialdehyde (MDA) determination, the experimental method was followed with slight modifications [24]. The specific operational steps are as follows: In a 10 mL graduated test tube with a stopper, add 1 mL of supernatant (same as used for antioxidant enzyme assay), then add 2 mL of 0.67% thiobarbituric acid solution. For the blank control, use an equal volume of distilled water instead.

Boil the samples in a 100 °C water bath for 15 min, then rapidly cool them. Centrifuge the samples at 7000 rcf for 10 min using a high-speed centrifuge. Take 200 µL of the supernatant and load it into clean and uncontaminated enzyme-specific fluorescence plate wells. Measure the optical density (OD) values at wavelengths of 450 nm, 532 nm, and 600 nm. Calculate using the formula: C_{MDA} (µmol/L) = 6.45 × ($A_{532\,nm}$ − $A_{600\,nm}$) − 0.56 × $A_{450\,nm}$.

For relative electrical conductivity determination, three replicates were taken from each plant, with 0.1 g of leaves cut from each. The leaves were washed thoroughly with tap water and then rinsed 2–3 times with ddH_2O. Excess water on the leaves was blotted dry with absorbent paper. The cleaned leaves were completely immersed in a centrifuge tube filled with 10 mL of distilled water. The tube was placed in a vacuum-drying oven and evacuated for 30 min until the leaves settled at the bottom. The tube was then placed in a constant temperature incubator at 25 °C for 1 h, with shaking every twenty minutes. The conductivity R1 was measured with the tube being maintained at 25 °C. The tube was placed in boiling water for 20 min. After cooling to 25 °C, the conductivity R2 was measured. The formula for relative conductivity is as follows: Relative conductivity = R1/R2 × 100%.

2.6. Scanning Electron Microscopy Observation

The WT and *nwd* mutant plant leaves at the three-leaf stage were fixed in a formaldehyde acetic acid–ethanol (FAA) solution consisting of 3.7% (*v*/*v*) formaldehyde, 5% (*v*/*v*) acetic acid, and 50% (*v*/*v*) ethanol for 24 h at 4 °C. Following this, the leaves were dehydrated using an ascending series of ethanol concentrations (45%, 55%, 65%, 75%, 90%, 96%, and 100%). Critical drying was carried out using a Leica EM CPD030 desiccator (Leica Microsystems, Shanghai, China), and a layer of gold–palladium was applied to the samples using a Hitachi E-1045 ion sputter and carbon coating unit (Hitachi, Tokyo, Japan). Finally, examination of the prepared samples was performed using a JSM-IT500LA SEM (JEOL, Tokyo, Japan).

2.7. BSA-Seq Analysis of nwd Locus

For BSA-seq analysis, pools of *nwd* mutant (glabrous) and wild-type-like (normal) plants were created from F_2 individuals selected based on their precise phenotypic characteristics. Each pool consisted of 30 F_2 individuals mixed in equal proportions. Individually prepared and sequenced using the Illumina PE150 platform, these pools, together with the parental pools (*nwd* and HB), underwent SNP and InDel analysis across multiple samples utilizing the unified genotyping module in GATK3.8 software. This was followed by Variant Filtration to refine the population VCF file [25]. ANNOVAR (V1.1.0) software was used for variant site annotation, identifying genes and types of variations [26]. Subsequently, homozygous variant sites unique to each parent were selected as references, and the index values of the two offspring pools were computed. Average indices within each window were calculated to pinpoint candidate intervals.

2.8. RNA Extraction and qRT-PCR

RNA extraction was performed on true leaves at the three-leaf stage using the MiniBEST Plant RNA extraction kit (TaKaRa). The extracted RNA was then subjected to cDNA synthesis using M-MLV (RNase H2) reverse transcriptase (TaKaRa). For quantitative real-time PCR (qRT-PCR), the Roche LightCycler 480 (LC480) system was utilized with Universal SYBR Green qPCR Premix (Share-bio, Shanghai, China). The $2^{-\Delta\Delta Ct}$ method was employed to determine the relative expression levels of the target genes, with EFIA serving as the internal reference gene [27]. Primer details are provided in Table S2.

2.9. RNA-Seq Analysis

For RNA-seq analysis, the first true leaves from the wild-type and *nwd* mutant plants were individually harvested. Total RNA extraction from each biological replicate was performed using the MiniBEST Plant RNA extraction Kit (Takara). Each sample utilized 1 µg of RNA for subsequent library preparation. Following cluster formation, all 6 samples

were sequenced on the DNBSEQ platform, generating an average of 6.4 Gb of data per sample. Data filtering was conducted using SOAPnuke (BGI, Shanghai, China), involving the removal of reads containing adapters, elimination of reads with more than 5% unknown base content (N), and discarding low-quality reads. The resulting clean reads were aligned to the reference genome using HISAT (V2.1.0) for genome alignment and Bowtie2 (V2.4.4) for alignment to the reference gene sequence. Expression levels of genes and transcripts were quantified using RSEM (V1.3.1). Differentially expressed genes (DEGs) were determined by applying a minimum threshold of a 2-fold change in expression levels ($|\log2\ FC| \geq 1$) and an adjusted false discovery rate (FDR) ≤ 0.05.

2.10. Statistical Analysis and Flowchart

The data were analyzed using ImageJ (V1.8.0) software. Descriptive statistics were computed to summarize the demographic and clinical characteristics of the study population. To test the primary hypothesis, a two-sample *t*-test was used to compare the means of the continuous outcome variable between the two groups. Data were presented as mean ± SD, and statistical analysis was conducted using SPSS 20.0 software (SPSS, Chicago, IL, USA) with three biological replicates. A significance level of $p < 0.05$ was established to assess statistical significance.

The flowchart of the experimental design is shown in Figure 1.

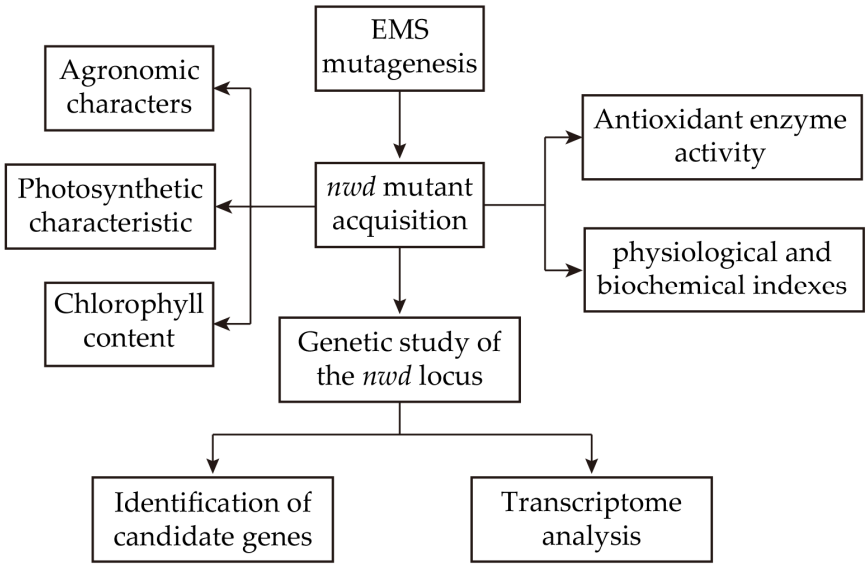


Figure 1. Flowchart of the experimental design.

3. Results

3.1. The EMS Mutant nwd Produced a Glabrous Phenotype

The *nwd* mutant was acquired from an M2 family derived from an EMS-mutagenized cucumber HB population. The wild-type HB plants were covered by trichomes on their leaves, female flowers, male flowers, tendrils, stems, and fruits (Figure 2A–F), while no trichomes could be observed on the *nwd* (Figure 2G–L).

To characterize the trichome morphology in detail, we observed trichomes with scanning electron microscopy (SEM), using the first true leaves of the *nwd* mutant and HB plants at the three-leaf stage. The results revealed notable differences between the smooth surface of the *nwd* leaves and the distinct characteristics of the trichomes observed on the HB leaves (Figure 3).

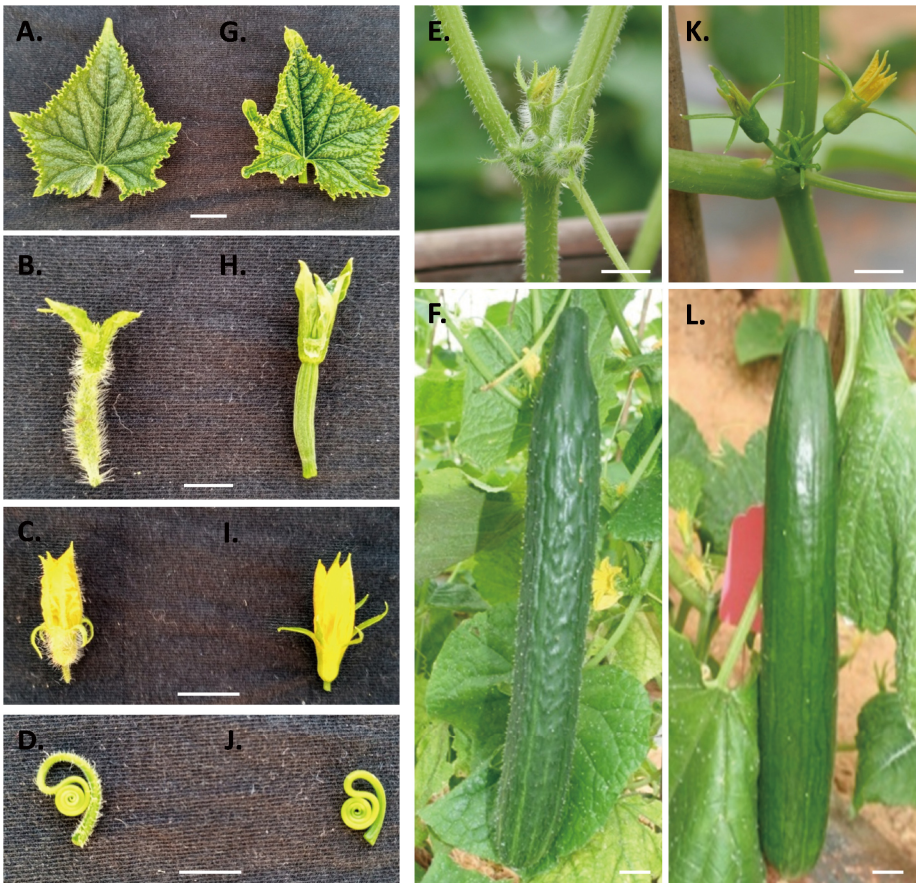


Figure 2. Trichome phenotypic characterization of leaf, female flower, male flower, tendril, stem, and fruit of wild-type HB (**A**–**F**) and *nwd* mutant (**G**–**L**). All pictures were taken at the maturation stage. Bars = 1 cm.

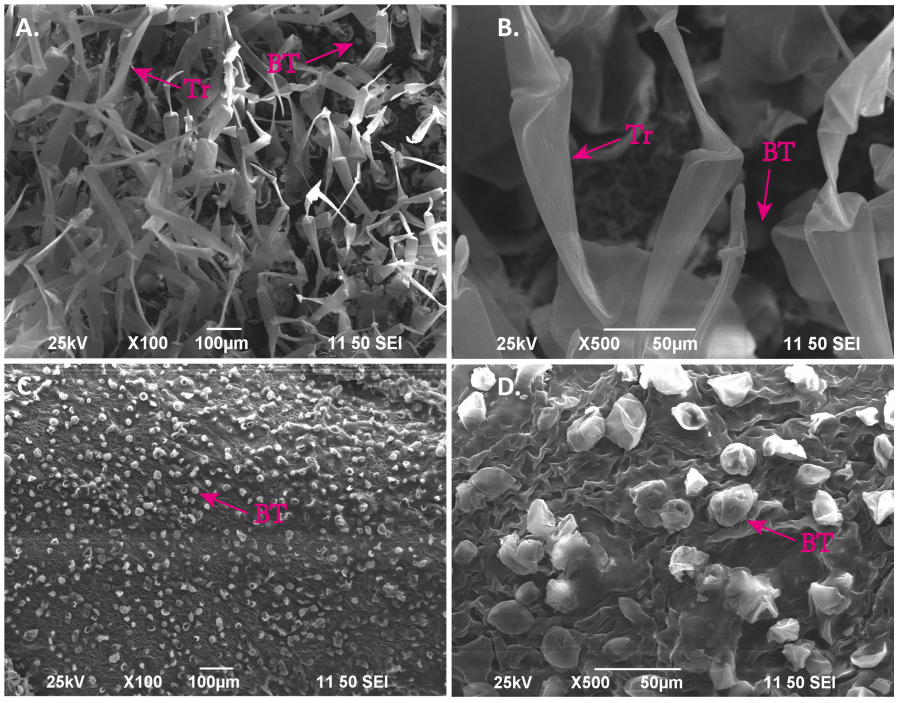


Figure 3. SEM images of the epidermis of the first true leaves at the three-leaf stage from WT (**A**,**B**) and the *nwd* (**C**,**D**). Tr, trichome; BT, bloom trichome.

3.2. Inheritance of the nwd Locus

We crossed the HB with the *nwd* to construct a segregation population, and the results showed that all 11 F_1 individuals were non-glabrous like the HB plants (Table 1). The 106 individuals of the BC_1P_2 population from a cross between the F_1 and *nwd* were observed as having 55 non-glabrous plants and 51 glabrous plants, while the whole BC_1P_1 population (F_1 × HB) was non-glabrous. In the F_2 population, the non-glabrous and glabrous individuals were segregated at an approximate rate of 3:1 (115 non-glabrous: 37 glabrous; $\chi^2 = 1.14$; $p > 0.05$). These results show that *nwd* is conferred by a single recessive gene.

Table 1. Separation ratios of WT HB and *nwd* in F_1 and F_2 generations.

Population	Total Plant	Trichomes	Glabrous	Theoretical Ratio
P_1 (HB)	11	11	/	/
P_2 (*nwd*)	11	/	11	/
F_1	11	11	/	/
F_2	152	115	37	3:1
BC_1P_1 (F_1 × HB)	106	106	/	/
BC_1P_2 (F_1 × *nwd*)	106	55	51	1:1

3.3. Determination of Major Agronomic Traits, Photosynthetic Characteristics, and Chlorophyll Content of nwd

The primary agronomic traits of wild-type HB and *nwd* were measured during the seedling, vine extension, and maturity stages, including the plant height, leaf length, leaf width, petiole length, and stem diameter. During the vine extension and maturity stages, the *nwd* mutant displayed significant variations in plant height compared to the wild-type HB, while no significant differences were observed in other agronomic traits including the leaf length, leaf width, petiole length, and stem diameter (Figure 4). These results indicated that the primary agronomic traits of *nwd* had no differences in most agronomic traits from the wild-type.

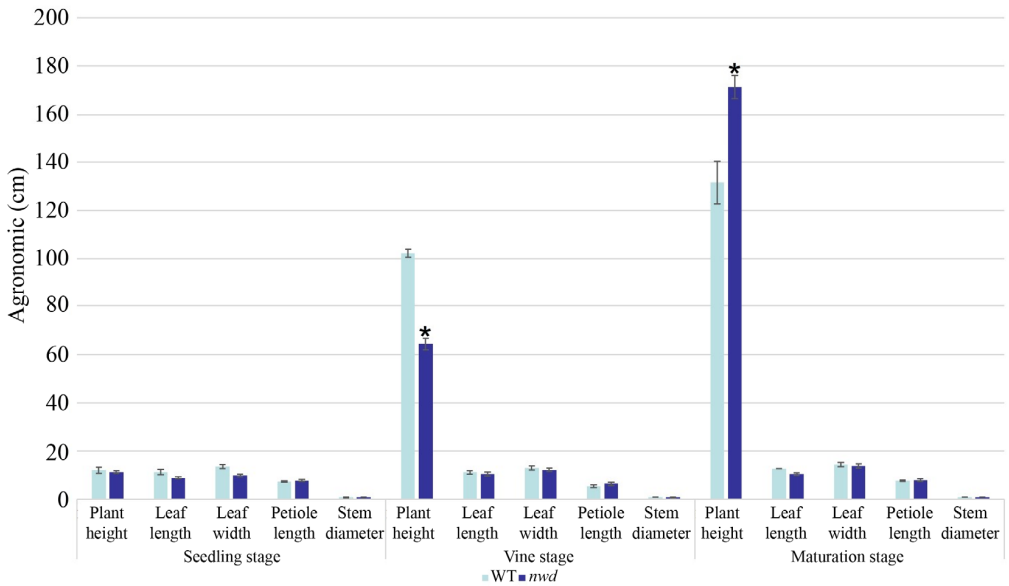


Figure 4. Agronomic properties of WT and *nwd* mutant plant. The plant height, leaf length, leaf width, petiole length, and stem thickness of the WT and *nwd* mutant plant were measured during the seedling, vine extension, and maturity stages. * $p < 0.05$ (*t*-test compared to wild-type values).

The net photosynthetic rate and transpiration rate during the vine extension stage in both wild-type HB and *nwd* were measured. As shown in Figure 5A, the *nwd* mutant exhibited a significantly lower net photosynthetic rate compared to wild-type HB, decreasing

from 30.07 μm/m^2/s to 24.37 μm/m^2/s. Changes in net photosynthetic rate may correlate with variations in plant photosynthetic pigments. Therefore, we also measured their chlorophyll content. Figure 5B demonstrates that chlorophyll a in *nwd* was significantly lower than in wild-type HB during both seedling and vine extension stages, while chlorophyll b and carotenoids showed no significant differences. The results indicated that the decrease in chlorophyll a in the *nwd* mutant may have led to a decrease in its photosynthesis efficiency.

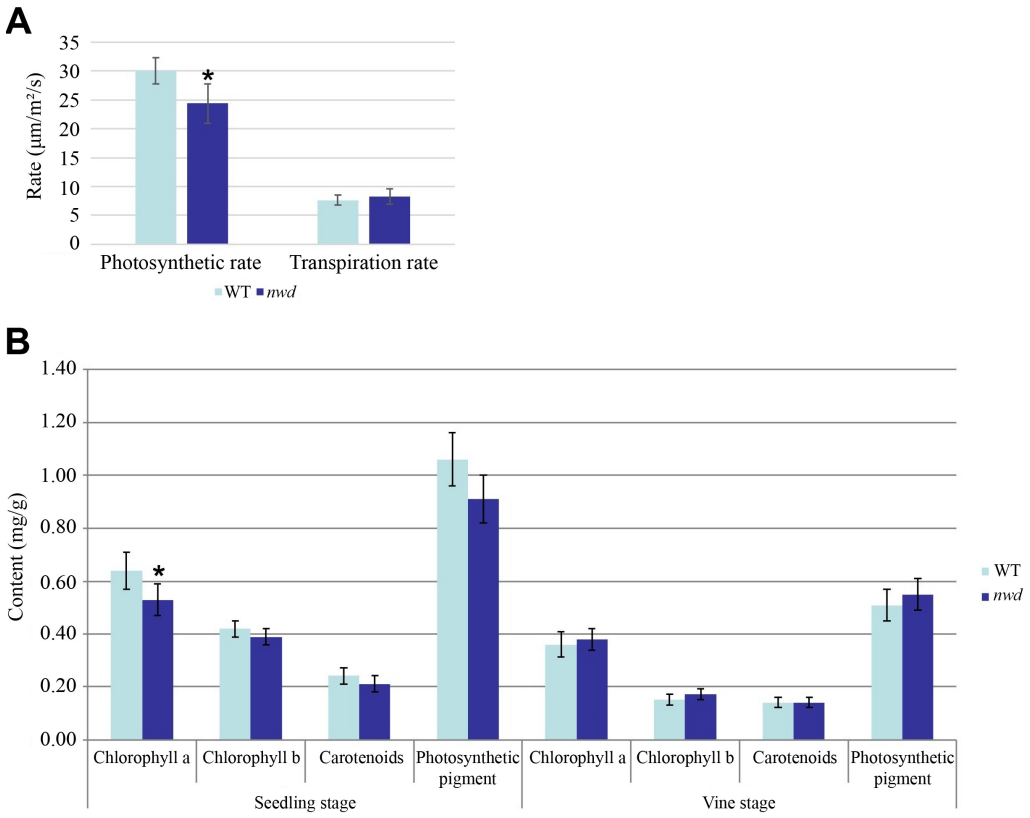


Figure 5. Photosynthetic characteristics and chlorophyll content of WT and *nwd* mutant plant. (**A**) The photosynthetic rate and transpiration rate of WT and *nwd* were measured using the true leaves from the same development stage. (**B**) Content of chlorophyll a, chlorophyll b, carotenoids, and photosynthetic pigment in *nwd* and WT. Samples were taken from the true leaves at the same development stage. * $p < 0.05$ (*t*-test compared to WT values).

3.4. Changes in Antioxidant Enzyme Activity, Soluble Protein Content, and Malondialdehyde Content in nwd

To understand whether mutations in the *NWD* gene affect antioxidant enzyme activity in cucumbers, we measured the activities of CAT, SOD, and POD in the leaves of wild-type HB and *nwd* during the seedling and vine stages. As shown in Figure 6A, during the seedling stage, *nwd* exhibited significantly lower CAT and SOD activities compared to the wild-type HB, but by the vine stage, their activities did not differ significantly between the wild-type HB and *nwd*. The soluble protein content, malondialdehyde (MDA) content, and relative conductivity were also measured. The results indicate that the soluble protein content in the *nwd* was significantly lower than in the wild-type HB during the vine stage (Figure 6B), while the MDA content was significantly higher in the *nwd* compared to the wild-type, regardless of the seedling or vine stage (Figure 6C). Thus, we concluded that the *nwd* mutant showed reduced antioxidant enzyme activity and lower soluble protein content compared to the wild-type during specific growth stages, with MDA was consistently higher in the *nwd* across both stages.

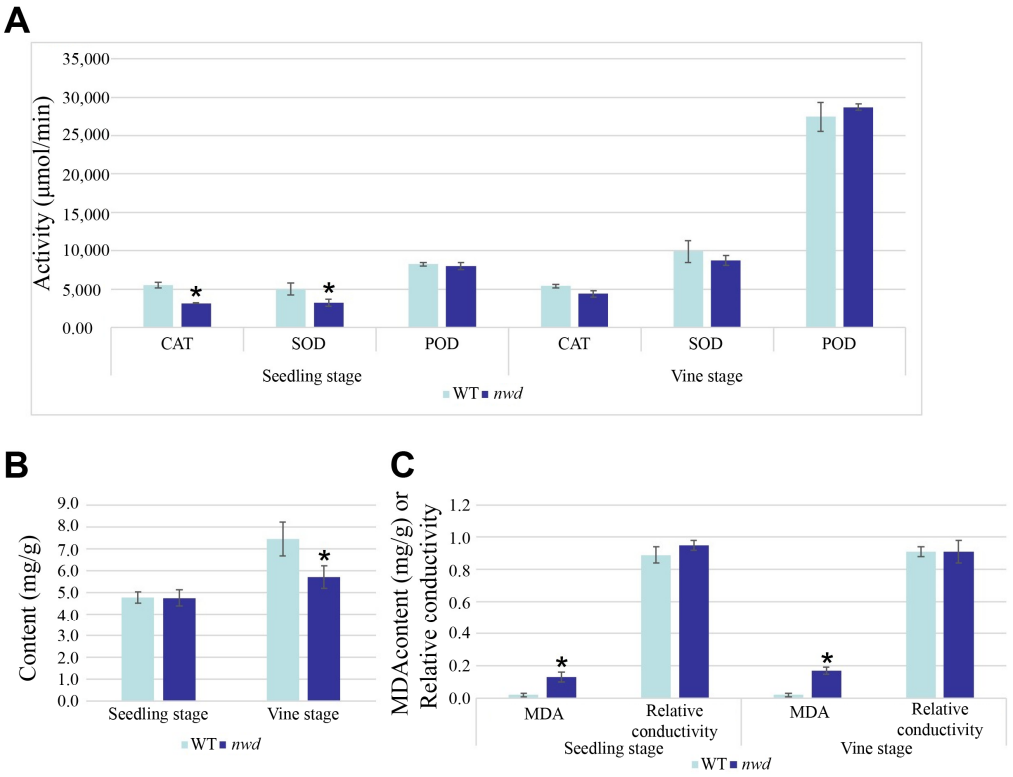


Figure 6. The antioxidant enzyme activity, relative conductivity, and soluble protein and malondialdehyde content of WT and *nwd* mutant plants. (**A**) The CAT, SOD, and POD activities in leaves of wild-type HB and *nwd* during the seedling and vine stages. (**B**) The soluble protein content in the *nwd* and HB during the seedling and vine stages. (**C**) The MDA content and relative conductivity in the *nwd* and HB during the seedling and vine stages. Samples were taken from the true leaves at the same development stage. * $p < 0.05$ (*t*-test compared to WT values).

3.5. Identification of Candidate Genes for nwd Mutant

To pinpoint the target gene, the Mutmap approach was employed, sequencing pooled samples of 30 mutants with distinct glabrous phenotypes from the F_2 segregating population, alongside 30 individuals exhibiting wild-type non-glabrous phenotypes. The SNPs and InDels across multiple samples, focusing on variant sites exhibiting homozygous differences between the parents, were detected. The results indicated that under a 99% threshold, only one candidate region was identified, located on the long arm of chromosome 3, spanning from 27,502,816 to 31,997,942 bp with a length of 4,495,126 bp (Figure 7A,B). Subsequently, using the F_2 population derived from the cross between the self-pollinated line HN and *nwd*, marker selection was conducted. Finally, the candidate region was successfully refined, spanning from markers InDel3-25 to InDel3-35, which corresponds to the genomic positions 25,244,673 and 5,015,454 (Figure 7C).

The re-sequencing results showed that the exonic mutations SNP27927016 (T-A; Trp-Arg), SNP28107578 (T-C; Glu-Gly), and SNP28111797 (G-A; Ser-Asn) within the above region resulted in changes in amino acids. To further confirm the candidate genes, we conducted gene-typing on an F_2 population constructed from crosses between 172 wild-type HN and *nwd* plants, revealing that these three mutation sites segregated with the glabrous phenotype (Figure 7C). Since the typical type of EMS mutation should be from G to A or from C to T, only the SNP28111797 (C-T; Ser-Asn) with an SNP index of one was screened. Based on the cucumber genome database v3 (http://cucurbitgenomics.org/organism/20 (accessed on 30 June 2024)) and gene annotation results, SNP28111797 is located within the gene *CsaV3_3G032590*, encoding a vacuolar protein sorting-associated protein. The findings indicate that *CsaV3_3G032590*, which harbors SNP28111797, is a candidate gene associated

with the *nwd* mutant in cucumber. In this study, this candidate gene was designated as *CsNWD*, referring to the cucumber glabrous mutant.

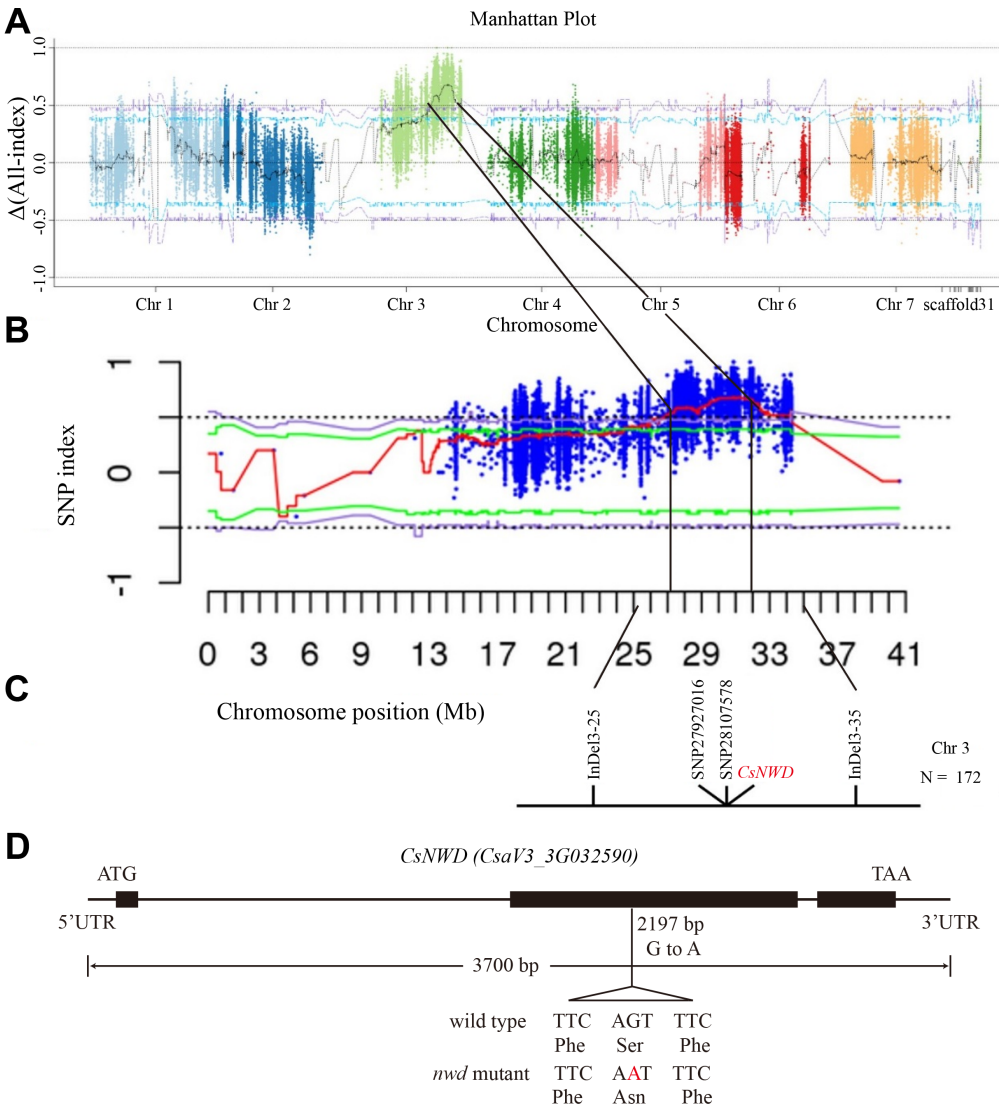


Figure 7. Mutmap and segregation for mapping glabrous locus, and the structure diagram of the *CsNWD* gene. (**A**) The distribution of Δ(All-index) across the seven chromosomes is depicted in two pools. Each point on the graph represents a single SNP site, with different colors representing different chromosomes. The SNP-index mean line is shown in black, the 95% threshold line in blue, and the 99% threshold line in purple. (**B**) The distribution of Δ(All-index) on chromosome 3 is presented for two pools, where each point represents an SNP site. The blue dots represent the SNP sites in chromosome 3. The SNP-index mean line is illustrated in red, while the 95% and 99% threshold lines are depicted in green and purple, respectively. (**C**) The genomic location of the *CsNWD* gene was determined to be on chromosome 3 using an F_2 population comprising 172 individuals derived from a cross between the inbred line HN and *nwd*. (**D**) The candidate gene *CsaV3_3G032590* exhibits a specific structure, with solid lines indicating introns and rectangles representing exons. In the *nwd* mutant, the mutated base is highlighted in red.

The *CsNWD* gene measures 3700 bp in length and includes three exons and two introns. Its coding sequence spans 1746 bp (Figure 7D). Within the second exon of the *CsNWD* gene, a transition from serine (Ser) to asparagine (Asn) at the 200th amino acid position was caused by a G to A substitution (Figure 7D). The qRT-PCR analysis revealed that the expression of *CsNWD* in the mutant remained unchanged compared to the wild-type (Figure 8A).

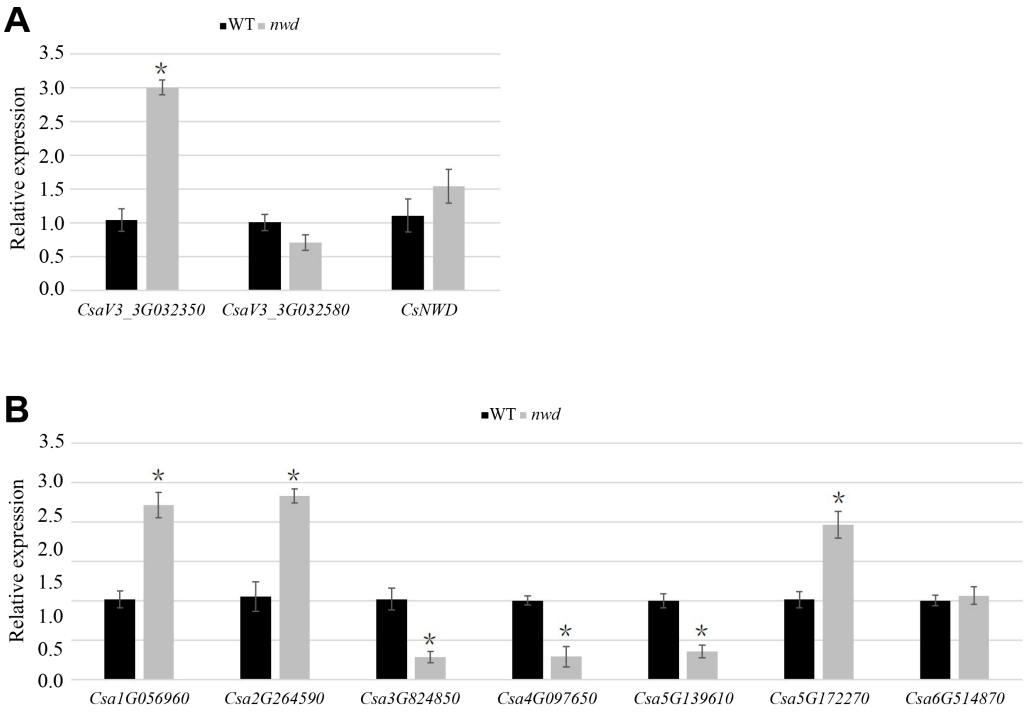


Figure 8. The relative expression level of candidate and reported genes in WT and *nwd* plants. (**A**) The relative expression level of *CsNWD*, *CsV3_3G032350*, and *CsV3_3G032580* in the true leaves of the *nwd* mutant; (**B**) The relative expression level of reported cucumber trichome genes in the *nwd* plant. The results represent the means ± SD. * $p < 0.05$ (*t*-test compared to wild-type values).

3.6. Quantitative Expression of Trichome-Related Genes in nwd

In order to investigate any alterations in *CsNWD* expression within the *nwd* mutant, a qRT-PCR analysis was conducted to measure the relative expression level. The findings indicate that there were no significant changes in *CsNWD* expression observed between the mutant and the wild-type (Figure 8A).

To preliminarily understand whether the target gene in the *nwd* mutant is associated with previously reported cucumber trichome genes, we quantitatively analyzed the expression of the *TS* (*Csa1G056960*), *NS* (*Csa2G264590*), *CsMYB6* (*Csa3G824850*), *TTG1* (*Csa4G097650*), *TRY* (*Csa5G139610*), *GA20ox1* (*Csa5G172270*), and *GL3/TRIL* (*Csa6G514870*) genes. The results showed differential expression of all genes except *GL3/TRIL* between the wild-type and *nwd* mutants (Figure 8B). Among these, the expression levels of the *TS*, *NS*, and *GA20ox1* genes were significantly higher in the *nwd* mutants, while the expression levels of the *CsMYB6*, *TTG1*, and *TRY* genes were significantly lower than in the wild-type (Figure 8B).

3.7. Comparative Transcriptome Analysis between nwd Mutant and Wild-Type

To further explore the possible molecular mechanisms of glabrous formation, we conducted transcriptome sequencing of wild-type and *nwd* mutant cucumber true leaves at the three-leaf stage using the Illumina HiSeq2000 platform. Sequences were annotated against the cucumber genome database v3 (http://cucurbitgenomics.org/organism/20 (accessed on 30 June 2024)) using BLAST. Differential gene expression between the wild-type and *nwd* mutants was determined using statistical parameters ($p < 0.05$; log2 > 2 or < −2). The results showed that 359 genes exhibited differential expression between the wild-type and *nwd* mutants, including 143 up-regulated and 216 down-regulated genes (Figure 9A).

To validate the differential expression of genes identified by transcriptomics, we selected three genes (*CsaV3_2G012160*, *CsaV3_2G035440*, and *CsaV3_6G042280*) for RT-qPCR analysis with three biological replicates. As shown in Figure 9B, the RT-qPCR results

were consistent with the trends observed in the transcriptomic data, indicating that our transcriptomics dataset provides a reliable reference for further studies.

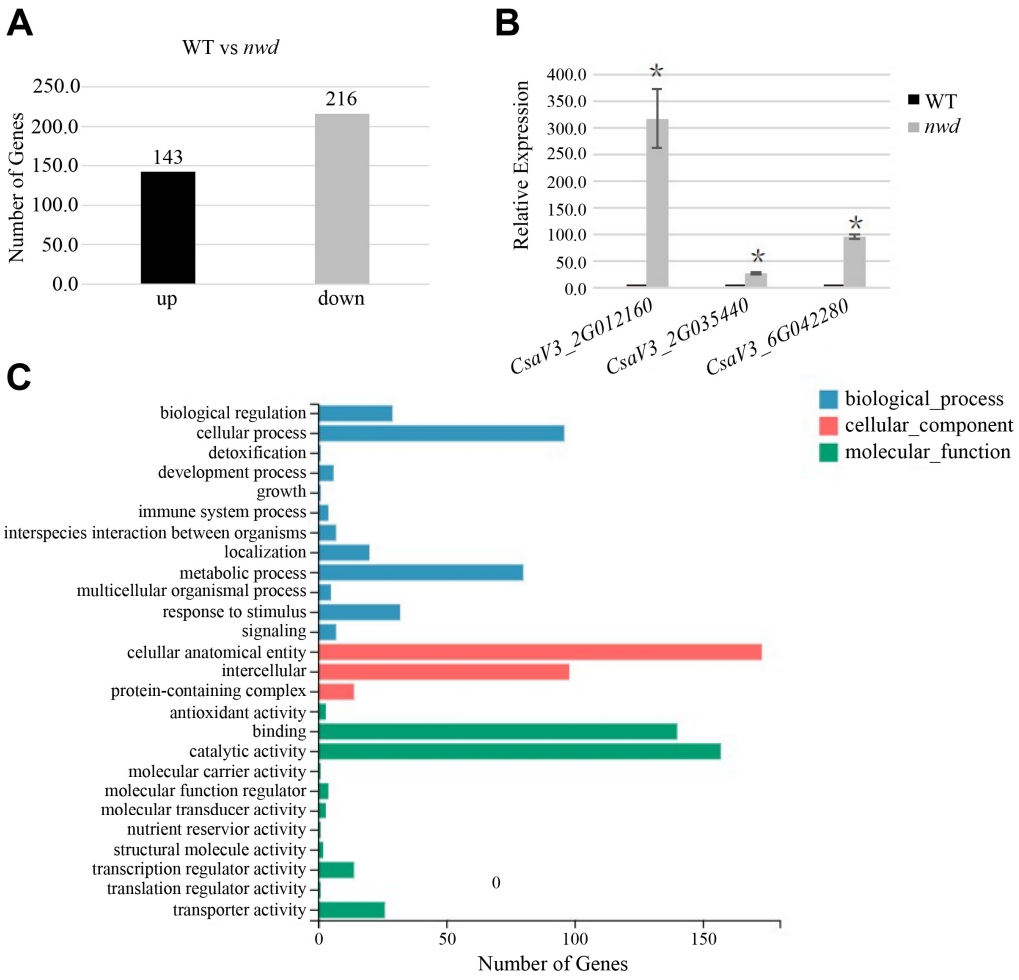


Figure 9. Differential gene expression analysis in WT and *nwd* plants. (**A**) Number of differential expression genes. (**B**) The selected 3 genes for RT-qPCR and their expression levels are consistent with the transcriptomic data trends. * $p < 0.05$ (*t*-test compared to wild-type values). (**C**) GO enrichment analysis of differentially expressed genes in WT and *nwd* plant. * $p < 0.05$ (*t*-test compared to wild-type values).

In order to investigate the biological functions of these genes with differential expression, a gene ontology (GO) analysis was performed. The mutant *nwd* was particularly enriched in the "cellular anatomical entity" cluster among all 26 GO terms, with 173 genes showing differential expression: 68 up-regulated genes and 105 down-regulated genes. Additionally, significant enrichment was observed in the "catalytic activity" cluster (53 up-regulated genes, 104 down-regulated genes), "binding" cluster (68 up-regulated genes, 72 down-regulated genes), under molecular function, and the "cellular process" cluster (39 up-regulated genes, 57 down-regulated genes) and "metabolic process" cluster (31 up-regulated genes, 49 down-regulated genes), under biological processes (Figure 9C).

In addition, an analysis was conducted to classify and determine the enrichment of 359 differentially expressed genes between the wild-type and *nwd* mutant using the KEGG database. This analysis aimed to identify the specific biological pathways in which these genes are involved. The results showed that these genes belonged to 19 KEGG categories across seven branches (Figure 10A), with the highest enrichment observed in the global and overview maps of metabolism, comprising 83 differentially expressed genes. Moreover, these genes were significantly enriched in the plant–pathogen interaction

pathway (23 genes), "RNA degradation" pathway (15 genes), and "Carbon metabolism" pathway (13 genes) (Figure 10B).

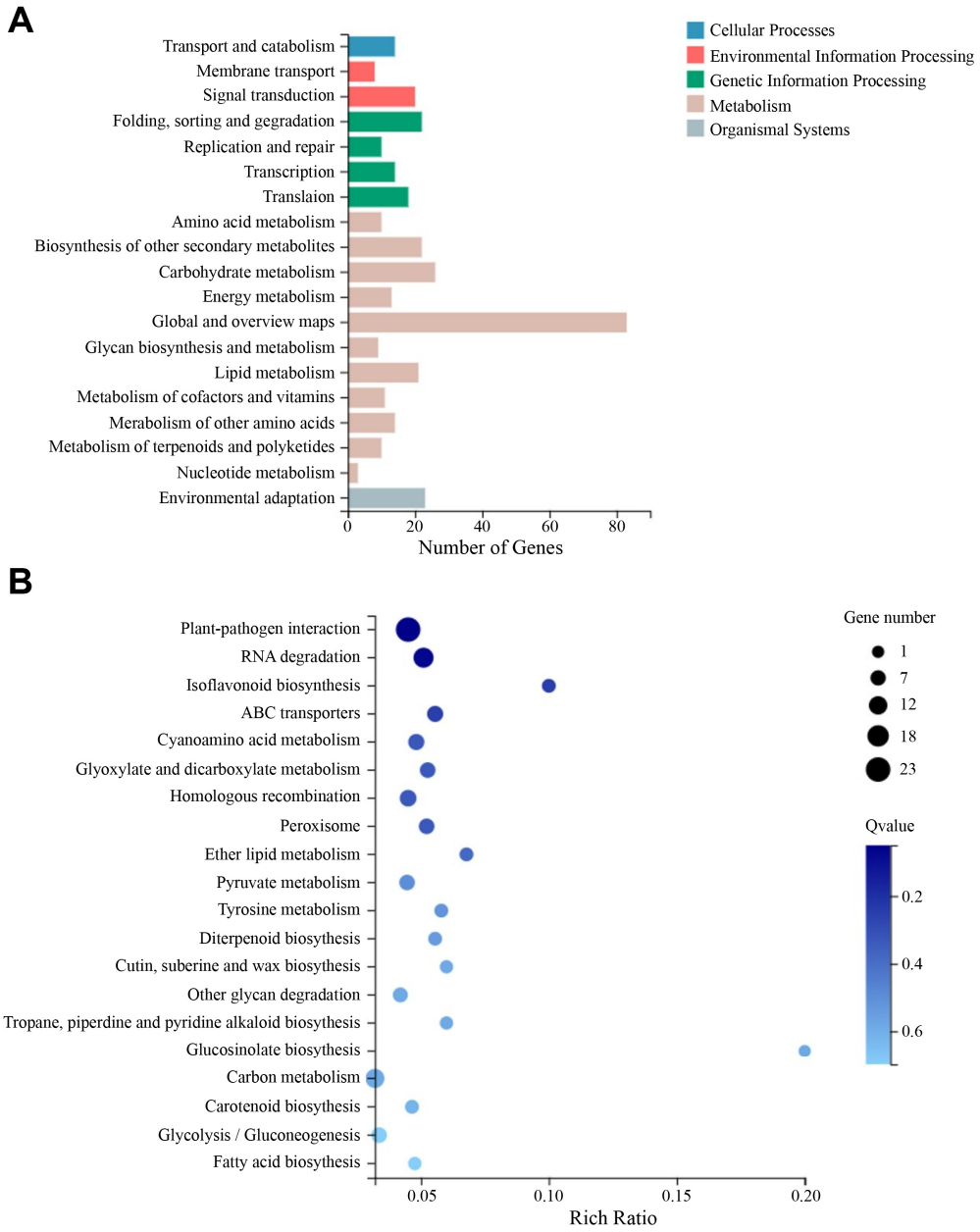


Figure 10. KEGG enrichment analysis of differentially expressed genes in WT and *nwd* plants. (**A**) KEGG classification and enrichment analysis of 359 differentially expressed genes between wild-type and *nwd* mutant in cucumber. (**B**) KEGG classification and enrichment analysis of 83 differentially expressed genes in "Global and overview maps".

Subsequently, based on the principle of significant differential expression, transcription factors, and homologous genes with reported functions, we selected 12 differentially expressed genes (*CsaV3_1G001170*, *CsaV3_1G038040*, *CsaV3_2G001750*, *CsaV3_3G034340*, *CsaV3_3G048280*, and *CsaV3_5G008510* down-regulated; *CsaV3_1G005440*, *CsaV3_3G032350*, *CsaV3_3G040820*, *CsaV3_4G023490*, *CsaV3_6G008810*, and *CsaV3_7G026200* up-regulated) for RT-qPCR analysis. As shown in Figure 11, their expression levels differed significantly between the cucumber wild-type and *nwd*. Interestingly, three genes (*CsaV3_2G001750*, *CsaV3_3G034340*, and *CsaV3_5G008510*) were nearly non-expressed in the *nwd*, but were

highly expressed in the wild-type material (with FPKM values of 26.6, 221.7, and 87.5, respectively) (Figure 11).

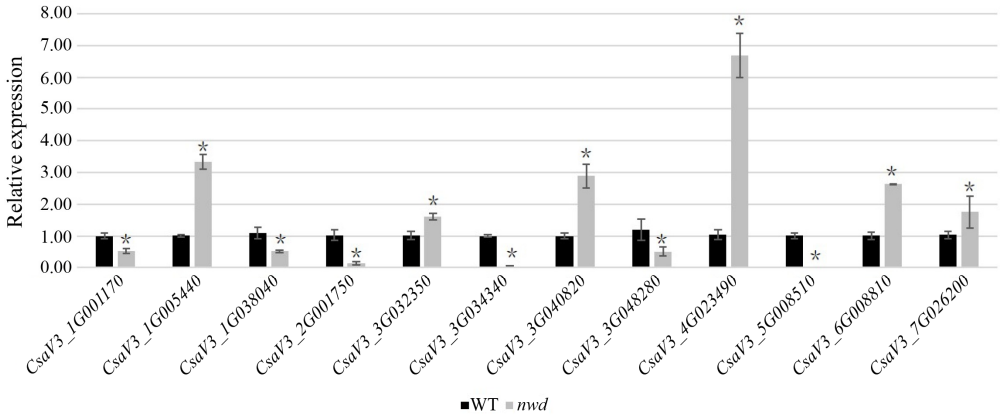


Figure 11. The relative expression level of candidate genes associated with trichome development in WT and *nwd* plant. * $p < 0.05$ (*t*-test compared to wild-type values).

4. Discussion

In plants, various glabrous mutations were reported, but their mutation mechanisms and the molecular understanding of the responsible loci remains unknown at present. Hair development in Arabidopsis has been extensively studied. It has been demonstrated that transcription factors and hormone actions play crucial roles in this developmental process [26]. The transcriptional activation by regulatory complexes composed of *GLABRA1* (*GL1*) [28], *TRANSPARENT TESTA GLABRA1* (*TTG1*) [29], and *GLABRA3*/*ENHANCER OF GLABRA3* (*GL3*/*EGL3*) [30,31] is critical for the initiation of hair formation.

Unlike the regulatory mechanisms of single-cell trichomes in Arabidopsis or Cotton, multicellular trichomes also involve plant-specific genes responsible for functional differentiation. An interesting example is the cotton gene *GaMYB2*, which shares homology with Arabidopsis *GL1* and plays a crucial role in regulating cotton fiber development. Remarkably, *GaMYB2* has the ability to rescue the phenotype of the Arabidopsis *gl1* mutant [32]. Similarly, *GaHOX1*, a cotton gene exhibiting homology with Arabidopsis *GL2*, has the capability of rescuing the phenotype observed in the Arabidopsis *gl2* mutant [33]. This discovery suggests that both cotton and Arabidopsis employ analogous transcription factors to regulate the development of single-cell trichomes. However, plants with multicellular trichomes appear to differ. For example, the *MIXTA* gene, a member of the *MYB* family, regulates snapdragon stigma development and, while unable to restore Arabidopsis *gl1* mutants, can control the differentiation of tobacco trichomes [34]. These results suggest that single-cell and multicellular epidermal hairs have distinct origins, their differentiation is controlled by different regulatory genes, and that homologous genes or proteins have specific functions that may differentiate in different plants.

In this study, we successfully identified and characterized a new cucumber glabrous mutant gene named *CsNWD*. Plants carrying the mutant gene exhibited glabrous leaves, stems, and fruits throughout their lifecycle. Genetic analysis of three glabrous mutants revealed that all F_1 progeny reverted to the wild-type phenotype with epidermal trichomes, indicating that *nwd* is a unique trichome development mutant in cucumber. Furthermore, we mapped the *CsNWD* gene in cucumber and identified the predicted candidate gene *CsaV3_3G032590*, which encodes a vacuolar protein sorting-associated protein (VPS protein). VPS proteins are involved in the sorting of soluble hydrolases and membrane proteins into vesicles destined for the lysosome-like vacuoles in yeast cells [35]. These proteins play a crucial role in recognizing and packaging cargo proteins into intraluminal vesicles (ILVs) within multivesicular bodies (MVBs). This process is essential for the proper degradation and recycling of cellular components [35,36]. This sorting process is also crucial for maintaining cellular homeostasis and responding to environmental changes by regulating the

turnover of proteins and organelles. The function of VPS proteins in plants involves similar roles to those in yeast, facilitating the sorting of proteins into vacuoles for degradation and recycling. Specifically, they aid in maintaining cellular homeostasis and responding to environmental cues by regulating protein and organelle turnover [37]. Studies linking VPS proteins directly to trichome fate determination and initiation are limited or absent in current research. It is worth noting that the Arabidopsis ESCRT (Endosomal Sorting Complex Required for Transport) components include several VPS proteins. For example, ESCRT-I comprises VPS23, VPS28, and VPS37 and ESCRT-II includes VPS22, VPS25, and VPS36 [38]. So far, the function of the ESCRT complex in plant cytokinesis has not been well established, although this function has been confirmed in mammals.

To investigate potential changes in the expression levels of transcription factors in the *nwd* mutant, we performed an analysis comparing differentially expressed transcription factors between wild-type and *nwd*. The results revealed a total of 14 transcription factors (Table S1), categorized into six groups: ethylene response (*CsaV3_3G012170*, *CsaV3_3G002470*, *CsaV3_6G013210*, *CsaV3_6G022740*, *CsaV3_3G030040*), *WRKY* (*CsaV3_2G032470*, *CsaV3_6G042280*, *CsaV3_2G017720*, *CsaV3_7G022650*), *MYB* (*CsaV3_2G028170*), *MYC* (*CsaV3_3G000850*), and other transcription factors (General transcription factor IIF subunit 2, *CsaV3_5G025800,* and JUNGBRUNNEN 1-like, *CsaV3_7G022730*). WRKYs are involved in the differentiation and development of trichomes in plants. For example, the Arabidopsis *WRKY* gene (*TTG2*) is highly expressed throughout the development of trichomes. *TTG2* acts downstream of the regulatory genes *TTG1* and *GLABROUS1*, similar to another key gene *GLABRA2*, playing a crucial role in regulating trichome formation in Arabidopsis [39].

Plant hormones are known to have a crucial role in the regulation of trichome development. Studies conducted previously demonstrate that short-term exposure to gaseous ethylene can induce cell division and influence the fate and polarity of trichomes, resulting in abnormal formation of guard cells and trichomes in cucumber plants [40]. In our transcriptomic data, we identified five ethylene-responsive genes (*CsaV3_3G012170*, *CsaV3_3G002470*, *CsaV3_6G013210*, *CsaV3_6G022740*, and *CsaV3_3G030040*) (Table S1). These plant hormone-related genes contribute to understanding the regulatory mechanisms of multicellular trichome development in cucumber.

In general, although we have currently identified candidate genes associated with the glabrous phenotype of the *nwd* mutant, it is essential to verify the accuracy of these candidate genes through complementation or gene-knockout experiments in subsequent steps. Additionally, further elucidation of the biological functions and molecular regulatory mechanisms of this gene through biological methods such as molecular biology, cell biology, and genetics will help deepen the understanding of the molecular mechanisms related to the development of cucumber trichomes.

5. Conclusions

In this study, we characterized an EMS-induced mutant known as *nwd*, which exhibited the glabrous phenotype. Comparative analysis with the wild-type revealed a significant reduction in photosynthetic capacity and chlorophyll a content in the *nwd* plants. Additionally, the mutant displayed notable changes in antioxidant enzyme activities, soluble protein levels, and malondialdehyde content. RNA-seq analysis indicated that the DEGs were primarily enriched in global metabolic pathways, overview maps of metabolism, and the plant–pathogen interaction pathway. The BSA-seq results identified *CsNWD* (*CsaV3_3G032590*) as the sole candidate gene, encoding a VPS protein. Overall, these findings contribute to a deeper understanding of the regulatory mechanisms underlying multicellular trichome development in cucumber. In addition, the discovery of the cucumber glabrous gene not only contributes to the cultivation of new varieties with reduced pesticide residues and enhanced pest resistance, but also offers significant genetic resources and tools for the molecular breeding and functional gene research of cucumbers.

Supplementary Materials: The following supporting information can be downloaded at: https://www.mdpi.com/article/10.3390/agronomy14092019/s1, Table S1: Transcription factors of differentially expressed genes identified by transcriptome; Table S2: Primers used in qRT-PCR.

Author Contributions: Conceptualization, S.L. and Y.Z. (Yuelong Zhou); Methodology, M.X. and Y.Z. (Yuelong Zhou); Software, M.X., Y.Z. (Yong Zhou) and Z.H.; Validation, M.X. and Y.Z. (Yuelong Zhou); Formal analysis, M.X. and Y.Z. (Yuelong Zhou); Data curation, Y.Z. (Yong Zhou), M.X. and Y.Z. (Yuelong Zhou); Writing—original draft preparation, Y.Z. (Yuelong Zhou) and Z.H.; Writing—review and editing, Y.Z. (Yuelong Zhou) and S.L.; Supervision, Z.H.; Project administration, S.L.; funding acquisition, S.L. and Y.Z. (Yuelong Zhou). All authors have read and agreed to the published version of the manuscript.

Funding: This research was funded by the National Natural Science Foundation of China (32160709 and 31860566), the Natural Science Foundation of Jiangxi Province, China (20232ACB205020, 20232BAB205013 and 20224BAB215024), and the earmarked fund for Innovation team of Jiangxi Agricultural University (JXAUCXTD009).

Data Availability Statement: The original contributions presented in the study are included in the article/Supplementary Materials; further inquiries can be directed to the corresponding author.

Conflicts of Interest: The authors declare that they have no conflicts of interest.

References

1. Dong, Y.; Li, S.; Wu, H.; Gao, Y.; Feng, Z.; Zhao, X.; Shan, L.; Zhang, Z.; Ren, H.; Liu, X. Advances in understanding epigenetic regulation of plant trichome development: A comprehensive review. *Hortic. Res.* **2023**, *10*, uhad145. [CrossRef] [PubMed]
2. Han, G.; Li, Y.; Yang, Z.; Wang, C.; Zhang, Y.; Wang, B. Molecular Mechanisms of Plant Trichome Development. *Front. Plant Sci.* **2022**, *13*, 910228. [CrossRef]
3. Huang, S.; Li, R.; Zhang, Z.; Li, L.; Gu, X.; Fan, W.; Lucas, W.J.; Wang, X.; Xie, B.; Ni, P.; et al. The genome of the cucumber, *Cucumis sativus* L. *Nat. Genet.* **2009**, *41*, 1275–1281. [CrossRef] [PubMed]
4. Hulskamp, M.; Schnittger, A.; Folkers, U. Pattern formation and cell differentiation: Trichomes in *Arabidopsis* as a genetic model system. *Int. Rev. Cytol.* **1999**, *186*, 147–178. [PubMed]
5. Hulskamp, M. Plant trichomes: A model for cell differentiation. *Nat. Rev. Mol. Cell Biol.* **2004**, *5*, 471–480. [CrossRef]
6. Pan, Y.; Bo, K.; Cheng, Z.; Weng, Y. The loss-of-function GLABROUS 3 mutation in cucumber is due to LTR-retrotransposon insertion in a class IV HD-ZIP transcription factor gene CsGL3 that is epistatic over CsGL1. *BMC Plant Biol.* **2015**, *15*, 302. [CrossRef]
7. Xue, S.; Dong, M.; Liu, X.; Xu, S.; Pang, J.; Zhang, W.; Weng, Y.; Ren, H. Classification of fruit trichomes in cucumber and effects of plant hormones on type II fruit trichome development. *Planta* **2019**, *249*, 407–416. [CrossRef] [PubMed]
8. Chen, C.; Liu, M.; Jiang, L.; Liu, X.; Zhao, J.; Yan, S.; Yang, S.; Ren, H.; Liu, R.; Zhang, X. Transcriptome profiling reveals roles of meristem regulators and polarity genes during fruit trichome development in cucumber (*Cucumis sativus* L.). *J. Exp. Bot.* **2014**, *65*, 4943–4958. [CrossRef]
9. Schuurink, R.; Tissier, A. Glandular trichomes: Micro-organs with model status? *New Phytol.* **2020**, *225*, 2251–2266. [CrossRef] [PubMed]
10. Karabourniotis, G.; Liakopoulos, G.; Nikolopoulos, D.; Bresta, P. Protective and defensive roles of non-glandular trichomes against multiple stresses: Structure–function coordination. *J. For. Res.* **2019**, *31*, 1–12. [CrossRef]
11. Weng, Y. *Cucumis sativus* Chromosome Evolution, Domestication, and Genetic Diversity: Implications for Cucumber Breeding. *Plant Breed. Rev.* **2021**, *44*, 79–111.
12. Li, Q.; Cao, C.; Zhang, C.; Zheng, S.; Wang, Z.; Wang, L.; Ren, Z. The identification of *Cucumis sativus* Glabrous 1 (CsGL1) required for the formation of trichomes uncovers a novel function for the homeodomain-leucine zipper I gene. *J. Exp. Bot.* **2015**, *66*, 2515–2526. [CrossRef] [PubMed]
13. Zhao, J.L.; Pan, J.S.; Guan, Y.; Zhang, W.W.; Bie, B.B.; Wang, Y.L.; He, H.L.; Lian, H.L.; Cai, R. Micro-trichome as a class I homeodomain-leucine zipper gene regulates multicellular trichome development in *Cucumis sativus*. *J. Integr. Plant Biol.* **2015**, *57*, 925–935. [CrossRef] [PubMed]
14. Pan, J.; Zhang, L.; Chen, G.; Wen, H.; Chen, Y.; Du, H.; Zhao, J.; He, H.; Lian, H.; Chen, H.; et al. Study of micro-trichome (mict) reveals novel connections between transcriptional regulation of multicellular trichome development and specific metabolism in cucumber. *Hortic. Res.* **2021**, *8*, 21. [CrossRef]
15. Wang, Y.-L.; Nie, J.-T.; Chen, H.-M.; Guo, C.-L.; Pan, J.; He, H.-L.; Pan, J.-S.; Cai, R. Identification and mapping of Tril, a homeodomain-leucine zipper gene involved in multicellular trichome initiation in *Cucumis sativus*. *Theor. Appl. Genet.* **2016**, *129*, 305–316. [CrossRef]
16. Du, H.; Wang, G.; Pan, J.; Chen, Y.; Xiao, T.; Zhang, L.; Zhang, K.; Wen, H.; Xiong, L.; Yu, Y.; et al. The HD-ZIP IV transcription factor Tril regulates fruit spine density through gene dosage effects in cucumber. *J. Exp. Bot.* **2020**, *71*, 6297–6310. [CrossRef] [PubMed]

17. Cui, J.-Y.; Miao, H.; Ding, L.-H.; Wehner, T.C.; Liu, P.-N.; Wang, Y.; Zhang, S.-P.; Gu, X.-F. A New Glabrous Gene (csgl3) Identified in Trichome Development in Cucumber (*Cucumis sativus* L.). *PLoS ONE* **2016**, *11*, e0148422. [CrossRef] [PubMed]
18. Yang, S.; Cai, Y.; Liu, X.; Dong, M.; Zhang, Y.; Chen, S.; Zhang, W.; Li, Y.; Tang, M.; Zhai, X.; et al. A CsMYB6-CsTRY module regulates fruit trichome initiation in cucumber. *J. Exp. Bot.* **2018**, *69*, 1887–1902. [CrossRef]
19. Yang, Z.; Song, M.; Cheng, F.; Zhang, M.; Davoudi, M.; Chen, J.; Lou, Q. A SNP Mutation in Homeodomain-DDT (HD-DDT) Transcription Factor Results in Multiple Trichomes (mt) in Cucumber (*Cucumis sativus* L.). *Genes* **2021**, *12*, 1478. [CrossRef]
20. Che, G.; Zhang, X. Molecular basis of cucumber fruit domestication. *Curr. Opin. Plant Biol.* **2019**, *47*, 38–46. [CrossRef]
21. Guo, P.; Chang, H.; Li, Q.; Wang, L.; Ren, Z.; Ren, H.; Chen, C. Transcriptome profiling reveals genes involved in spine development during CsTTG1-regulated pathway in cucumber (*Cucumis sativus* L.). *Plant Sci.* **2020**, *291*, 110354. [CrossRef] [PubMed]
22. Tauzin, A.S.; Giardina, T. Sucrose and invertases, a part of the plant defense response to the biotic stresses. *Front. Plant Sci.* **2014**, *5*, 293. [CrossRef] [PubMed]
23. Ulrike Oster, R.T.; Tanaka, A.; Rüdiger, W. Cloning and functional expression of the gene encoding the key enzyme for chlorophyll b biosynthesis (CAO) from *Arabidopsis thaliana*. *Plant J.* **2000**, *21*, 305–310. [CrossRef] [PubMed]
24. Suda, I.; Furuta, S.; Nishiba, Y. Fluorometric Determination of a 1,3-Diethyl-2-thiobarbituric Acid–Malondialdehyde Adduct as an Index of Lipid Peroxidation in Plant Materials. *Biosci. Biotechnol. Biochem.* **2014**, *58*, 14–17. [CrossRef]
25. Waters, B.M.; Chu, H.H.; Didonato, R.J.; Roberts, L.A.; Eisley, R.B.; Lahner, B.; Salt, D.E.; Walker, E.L. Mutations in *Arabidopsis* yellow stripe-like1 and yellow stripe-like3 reveal their roles in metal ion homeostasis and loading of metal ions in seeds. *Plant Physiol.* **2006**, *141*, 1446–1458. [CrossRef]
26. Wu, Z.; Zhang, X.; He, B.; Diao, L.; Sheng, S.; Wang, J.; Guo, X.; Su, N.; Wang, L.; Jiang, L.; et al. A chlorophyll-deficient rice mutant with impaired chlorophyllide esterification in chlorophyll biosynthesis. *Plant Physiol.* **2007**, *145*, 29–40. [CrossRef]
27. Livak, K.J.; Schmittgen, T.D. Analysis of Relative Gene Expression Data Using Real-Time Quantitative PCR and the $2-\Delta\Delta CT$ Method. *Methods* **2001**, *25*, 402–408. [CrossRef]
28. Oppenheimer, D.G.; Herman, P.L.; Sivakumaran, S.; Esch, J.; Marks, M. A myb gene required for leaf trichome differentiation in *Arabidopsis* is expressed in stipules. *Cell* **1991**, *67*, 483–493. [CrossRef]
29. Walker, A.R.; Davison, P.A.; Bolognesi-Winfield, A.C.; James, C.M.; Srinivasan, N.; Blundell, T.L.; Esch, J.J.; Marks, M.D.; Gray, J.C. The Transparent Testa GLABRA1 Locus, which Regulates Trichome Differentiation and Anthocyanin Biosynthesis in *Arabidopsis*, Encodes a WD40 Repeat Protein. *Plant Cell* **1999**, *11*, 1337–1349. [CrossRef]
30. Payne, C.T.; Zhang, F.; Lloyd, A.M. GL3 encodes a bHLH protein that regulates trichome development in *Arabidopsis* through interaction with GL1 and TTG1. *Genetics* **2000**, *156*, 1349–1362. [CrossRef]
31. Schena, M.; Davis, R.W. HD-Zip proteins: Members of an *Arabidopsis* homeodomain protein superfamily. *Proc. Natl. Acad. Sci. USA* **1992**, *89*, 3894–3898. [CrossRef] [PubMed]
32. Wang, S.; Wang, J.-W.; Yu, N.; Li, C.-H.; Luo, B.; Gou, J.-Y.; Wang, L.-J.; Chen, X.-Y. Control of Plant Trichome Development by a Cotton Fiber MYB Gene. *Plant Cell* **2004**, *16*, 2323–2334. [CrossRef] [PubMed]
33. Guan, X.Y.; Li, Q.J.; Shan, C.M.; Wang, S.; Mao, Y.B.; Wang, L.J.; Chen, X.Y. The HD-Zip IV gene GaHOX1 from cotton is a functional homologue of the *Arabidopsis* GLABRA2. *Physiol. Plant.* **2008**, *134*, 174–182. [CrossRef] [PubMed]
34. Payne, T.; Clement, J.; Arnold, D.; Lloyd, A. Heterologous myb genes distinct from GL1 enhance trichome production when overexpressed in *Nicotiana tabacum*. *Development* **1999**, *126*, 671–682. [CrossRef] [PubMed]
35. Bassham, D.C.; Raikhel, N.V. Unique features of the plant vacuolar sorting machinery. *Curr. Opin. Cell Biol.* **2000**, *12*, 491–595. [CrossRef]
36. Robinson, D.G.; Herranz, M.-C.; Bubeck, J.; Pepperkok, R.; Ritzenthaler, C. Membrane Dynamics in the Early Secretory Pathway. *Crit. Rev. Plant Sci.* **2007**, *26*, 199–225. [CrossRef]
37. Scheuring, D.; Viotti, C.; Kruger, F.; Kunzl, F.; Sturm, S.; Bubeck, J.; Hillmer, S.; Frigerio, L.; Robinson, D.G.; Pimpl, P.; et al. Multivesicular Bodies Mature from the Trans-Golgi Network/Early Endosome in *Arabidopsis*. *Plant Cell* **2011**, *23*, 3463–3481. [CrossRef]
38. Gao, C.; Zhuang, X.; Shen, J.; Jiang, L. Plant ESCRT Complexes: Moving Beyond Endosomal Sorting. *Trends Plant Sci.* **2017**, *22*, 986–998. [CrossRef]
39. Johnson, C.S.; Kolevski, B.; Smyth, D.R. Transparent Testa GLABRA2, a Trichome and Seed Coat Development Gene of *Arabidopsis*, Encodes a WRKY Transcription Factor. *Plant Cell* **2002**, *14*, 1359–1375. [CrossRef]
40. Kazama, H.; Dan, H.; Imaseki, H.; Wasteneys, G.O. Transient Exposure to Ethylene Stimulates Cell Division and Alters the Fate and Polarity of Hypocotyl Epidermal Cells. *Plant Physiol.* **2004**, *134*, 1614–1623. [CrossRef]

Disclaimer/Publisher's Note: The statements, opinions and data contained in all publications are solely those of the individual author(s) and contributor(s) and not of MDPI and/or the editor(s). MDPI and/or the editor(s) disclaim responsibility for any injury to people or property resulting from any ideas, methods, instructions or products referred to in the content.